Journal of The Electrochemical Society, **161** (9) D447-D452 (2014)
0013-4651/2014/161(9)/D447/6/$31.00 © The Electrochemical Society

Artificially Controlled Two-Step Electrodeposition of Cu and Cu/In Metal Precursors with Improved Surface Roughness for Solar Applications

Yong Hun Kwon, Sung Kyun Kim, Sang-Woo Kim,* and Hyung Koun Cho[z]

School of Advanced Materials Science and Engineering, Sungkyunkwan University, Suwon 440-746, Korea

The very smooth surfaces of the multistacked metal layers fabricated by electrodeposition are particularly useful for obtaining the designed composition and the optimized composition distribution in CIGS solar cells. Thus, we employed an artificially controlled two-step electrodeposition method for the deposition of reproducible and smooth Cu layers on Mo substrates. First, the chronoamperometry at various applied potentials was investigated to confirm growth behavior at a direct constant potential. According to these results, a two-step process was designed: i) at the first step, high negative potential was applied for the formation of high density nuclei, and ii) at the second step, low negative potential was employed to promote the homogenous coalescence of the Cu nuclei. As a result, the root mean square (RMS) value of the Cu surface measured by atomic force microscopy was considerably decreased by up to 6.0 nm using the two-step process, compared to that fabricated using a single-step process. In addition, the relatively smooth In surface was observed on the Cu/In bilayers fabricated using the two-step process.
© 2014 The Electrochemical Society. [DOI: 10.1149/2.0771409jes] All rights reserved.

Manuscript submitted April 24, 2014; revised manuscript received May 27, 2014. Published June 17, 2014.

Thin film solar cells based on chalcogenide and kesterite materials such as CIGS, CdTe, and CZTS have emerged as principal renewable energy generation systems due to their cost effectiveness, light weight, and flexibility.[1–7] Among them, the $Cu(In_{1-x}Ga_x)Se_2$ (CIGS) is still a strong candidate as an absorber layer for thin film solar cells with high efficiency due to its high absorption coefficient ($> \sim 10^5$ /cm).[4] In addition, the band-gap of CIGS could be controlled by adjusting the Ga/In composition ratio in the CIGS films. Experimentally, it is known that high conversion efficiency in the CIGS films has been obtained when Ga/(In+Ga) is ~0.3.[1,8] To date, ZSW in Germany presented a CIGS cell efficiency of 20.8%, which is the highest thin film solar cell efficiency.[9] Despite such potential applications and results, issues remain such as the need to reduce the process and the element cost, and the need to develop a coating technology with reproducible and uniform composition distribution.

Until now, the above difficulties in the growth of the CIGS absorber have been addressed by utilizing the co-evaporation method and sputtering method.[1,2,8,9] However, these processes require high initial facility cost from a high vacuum condition and a superfluous consumption of raw materials, despite the methods used for mass production in various fields.[10–12] Alternatively, simple binary or ternary compounds with low cost such as SnS, Cu_2O, FeS_2, Zn_3P_2, Cu_2S, $ZnSn(N,P)_2$, and Cu_2SnS_3, etc. have been studied for developing novel inorganic semiconductor materials.[13–20] Additionally, non-vacuum processes have been considered as an emerging technology for CIGS coating, and are mainly based on solution approaches including electrochemical deposition, nanoparticle solution technique, and spray pyrolysis.[11,12,21–24] However, these solution processes incorporate undesired impurities related to carbon, oxygen, and chlorine from the precursor and solvent. Also, additional thermal treatment should be performed at high temperature for the crystallization and uniform composition distribution. Thus, it is difficult to state that a solution process can be applied to flexible devices, despite its many advantages. Among these solution processes, electrodeposition has been considered to be favorable method for low cost and high through-put. The electrodeposition can provide simple material design systems in multicomponent compounds and low capital for an initial set-up. In addition, the re-use and recycling of the electrodeposition solution is effectively possible.[11] Thus, some research groups have attempted to apply electrodeposition as an alternative process for the fabrication of CIGS solar cells.[11,12,25,26] Currently, electrodeposited CIGS solar cells with the conversion efficiency of 15.9% were reported by Nexcis (module efficiency of 12.2%).[2]

*Electrochemical Society Active Member.
[z]E-mail: chohk@skku.edu

Similar to the sputtering method with the limitation of Se incorporation, the electrodeposition also has a technical limitation regarding Se and Ga incorporation, due to the significant difference in appropriate applied potentials between metal precursors and the Se precursor. Thus, the coating of CIGS absorber layers has been prepared with multistacked layers or co-deposited precursors, but they mostly need an additional and complex selenization process.[26] In 2013, Duchatelet et al. reported a conversion efficiency of 12.4% from co-deposited precursors, and Bhattacharya et al. reported 11.7% from multistacked Cu/In/Ga precursors.[11,12] Even though the formation of CIGS precursors using a single bath is conceptually ideal, it is very difficult to grow as-deposited CIGS films with a designed stoichiometric composition in a one-step single bath system. This is attributed to the fact that the reduction potentials of Se and Cu are high, and those of In and Ga are quite negatively shifted.[26] This indicates that the formation of Cu-Se compounds is relatively easy, but In and Ga related selenide compounds show fairly different reaction rates, resulting in the additional selenization process with a delicately controlled recipe. The additional selenization process may induce inhomogeneous metal distribution and hinder the reproducible process.

On the other hand, the formation of multistacked metal precursors synthesized by the electrochemical reaction of metallic ions is a relatively simple and well developed process. After the precursor formation, the selenization process should be performed at a high temperature, similar to the sputtering based CIGS films. However, because the composition of metal elements is simply controlled by the thickness of each metal layer, high reproducibility is expected. Nevertheless, some single metal layers exhibit a rough surface compared to compound films, and also an underlying metallic layer in the multistacked structure has the role of a working electrode for the following growth.[27] In particular, the metal electrodeposition on the surface with a faceted roughness induces a relatively high current in the top region of the facets. This may be the origin of the non-uniform composition and the formation of unwanted phases such as Cu_2Se in the absorber layers after the selenization, which degrade the conversion cell efficiency and cause a high leakage current.[28] Therefore, the very flat and smooth surfaces of the Cu layers which were first deposited on the Mo substrates are very helpful for the formation of the optimized metal precursors in the CIGS solar cells fabricated by electrodeposition. In this study, we employed the electrodeposition for the multistacked metal precursors and an artificially controlled two-step electrodeposition method was suggested for the deposition of reproducible and smooth Cu layers on Mo substrates. Consequently, we demonstrate the usefulness of selecting a smooth Cu deposition for the Cu/In bilayer with appropriate surface roughness.

Downloaded on 2016-03-14 to IP 115.145.248.215 address. Redistribution subject to ECS terms of use (see ecsdl.org/site/terms_use) unless CC License in place (see abstract).

Experimental

In this study, we proposed a two-step electrodeposition method for the formation of the metal precursors with improved surface roughness. In the multistacked metal precursors for CIGS films fabricated by electrodeposition, the Cu layers were mainly selected as a first layer due to the controllability and the role of wetting layers on following metal layers. Firstly, to deposit the Cu layer, aqueous solution containing 0.1 M $CuSO_4$ and 0.1 M Na_2SO_4 was used as the electrolyte. Here, the pH of the solution was adjusted to 1 by sulfuric acid. For electrochemical deposition, a conventional three electrode system was employed, where Ag/AgCl and Pt foil were used as reference and counter electrodes, respectively. The glass substrates coated with the Mo layer with a 300 nm thickness were used as working electrodes, where the Mo was prepared by sputtering on soda lime glass. Before the deposition, Mo substrates were cleaned with acetone, ethanol, and deionized water in consecutive order for 10 min each in an ultrasonic bath. The native molybdenum oxide layer on the surface was etched with 25 vol% ammonia solution for 5 min, and then rinsed in DI water shortly before dipping in a electrolyte.[27]

To understand the deposition evolution of a Cu layer, chronoamperometry was monitored by a computationally controlled Versastat3 potentiostat system at −0, −50, −100, −200, −400, and −600 mV (vs Ag/AgCl). For the two-step electrodeposition, −600 and −800 mV were applied to the Mo substrates for a short period of time, 0.5 sec, to form the high density of nuclei at the first step, and the second step was then continuously performed at an applied potential of −100 mV. All Cu layers used were grown on Mo substrates until the cumulative charges reached 850 mC/cm^2, which corresponds to the thickness of ∼300 nm. Finally, the second In metal was deposited on the Cu layer grown at −100 mV using a two-step process to compare the effect of the surface roughness of the Cu layer on In deposition. The In deposition was performed in an aqueous solution containing 0.2 M $InCl_3$ and 0.1 M NaCl. The pH of the solution was around 3. After the deposition of each layer, optical microscopy and scanning electron microscopy (SEM) were used to confirm and characterize the surface morphology in large and small scales, respectively. Atomic force microscopy (AFM) in non-contact mode was employed to quantify the surface roughness of the Cu and Cu/In precursors in detail.

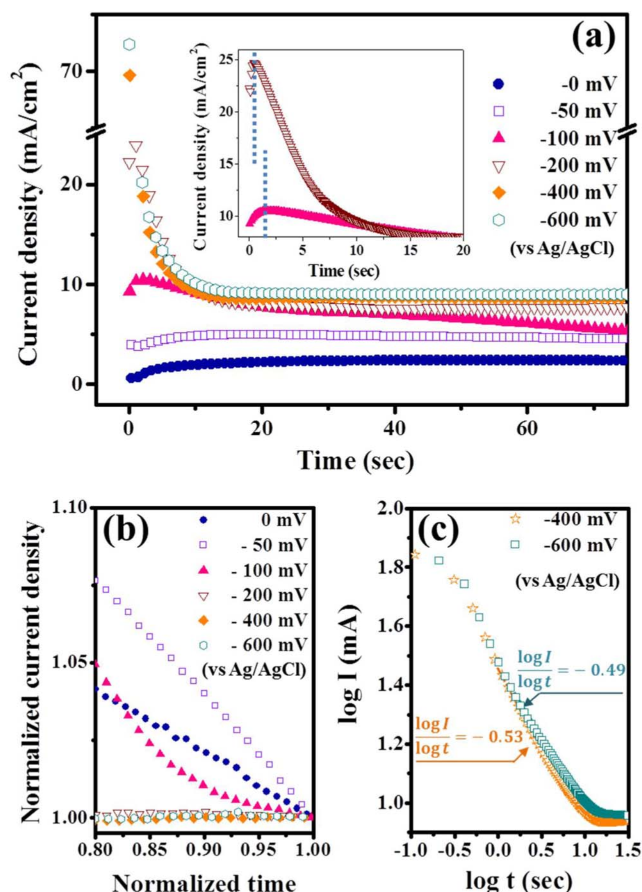

Figure 1. (a) Chronoamperometry and (inset) chronocoulometry results performed at various constant potentials (0, −50, −100, −200, −400, and −600 mV). (b) Chronoamperometry results normalized by the end values of each process. (c) Logarithmically transformed chronoamperometry results performed at −400 mV and −600 mV.

Results and Discussion

Figure 1a shows the variation of the potentiostatic current-time transient during Cu electrodeposition at each potential (0, −50, −100, −200, −400, and −600 mV). As shown in the inset of Fig. 1a, each potential was continuously applied to the Mo substrates until the total charge density reached 850 mC/cm^2, corresponding to ∼300 nm thickness. Generally, chronoamperometry curves can be classified into three stages: initial nucleation stage, transitional stage, and final stabilized stage. At the initial stage, the reduction current density is increased during nuclei germination. The current density is then rapidly dropped while nuclei coalesce with each other at the transitional stage. Finally, the current density is stabilized at a lower current density for the film growth.[29] According to the afore mentioned explanation, the increase of the reduction current was observed for a short period of time (<1 sec) under the applied potentials of −100 and −200 mV (initial nucleation stage), as shown in the inset of Fig. 1a. During the transitional stage, the current density was decreased at these potentials. Then, the stabilized current density with saturated values was also found for the final stage. Figure 1b shows the current-time transient normalized by the final values of the process. Here, the slope of the normalized current-time transient should be almost 0 at a normalized time of 1 for stabilized current density, but the slopes for the 0 and −50 mV potentials at a normalized time of 1 were not 0. This result indicates that the Cu layers in the applied potential of 0 and −50 mV were not fully coalesced, resulting in continuous films not being formed. Therefore, we found that the negative potential of > −50 mV should be applied for the preparation of the Cu films in this electrolyte. In addition, for the applied potentials of −400 and −600 mV, the increase of current density corresponding to the initial nucleation stage was not clearly detected due to the rapid nucleation rate, even though the transitional stage and final stage were distinguished.

Moreover, as shown in Fig. 1a, the saturated current density at 70 sec continuously increased due to the increase of negative potential. In particular, in the negative potential of ≥ −200 mV, significant changes in the level of current density were observed at this point, though the level of saturated current density was almost unchanged in the potential range of < −200 mV. In high Cu ion concentrations, Cu electrodeposition was not governed by the diffusion of reactants, and the reduction of current density increased with increasing negative potential.[29] Thus, our result probably indicates that the electrochemical reaction in ≥ −200 mV was governed by reaction kinetics. On the other hand, in the potential range of ≤ −400 mV, electrochemical reaction may follow a diffusion limited growth mechanism. To prove the diffusion controlled reaction in high negative potential, the following Cottrell equation, which is used for the heterogeneous system under diffusion control, was used.[30]

$$i\,(t) = \left(\frac{nFAD^{1/2}C_0^*}{\pi^{1/2}t^{1/2}}\right) \qquad [1]$$

where i, n, F, A, D, C_0, and t refer to the current, number of electrons, Faraday constant, area of the working electrode, diffusion coefficient, initial mole concentration of Cu, and time, respectively. As shown in Fig. 1c, the slopes of the logarithmically transformed current-time transient curves were −0.53 and −0.49 for the applied potentials of −400 and −600 mV, respectively. These values almost satisfy the

Downloaded on 2016-03-14 to IP 115.145.248.215 address. Redistribution subject to ECS terms of use (see ecsdl.org/site/terms_use) unless CC License in place (see abstract).

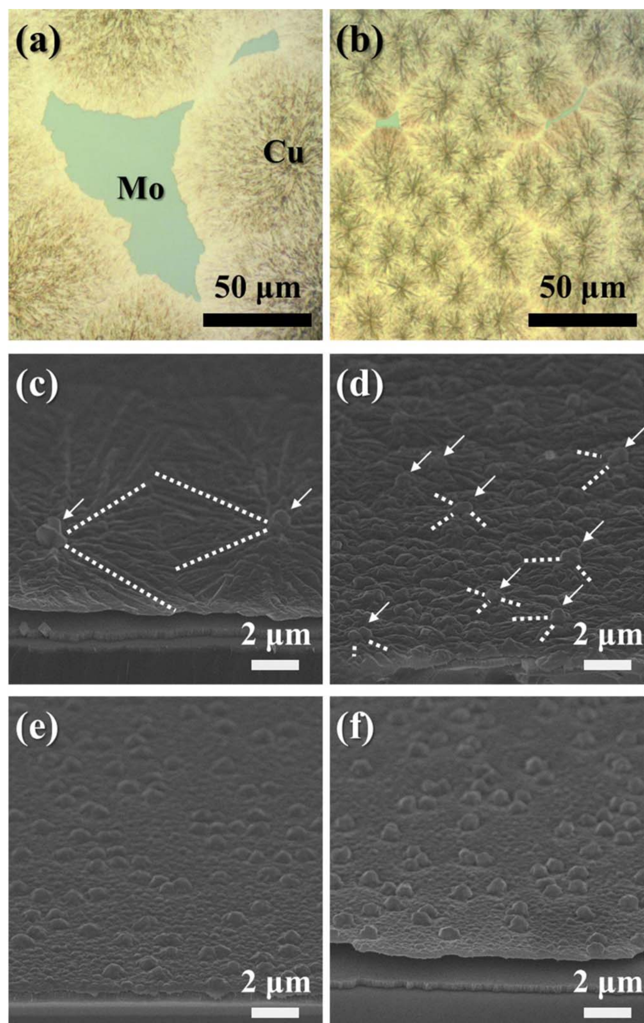

Figure 2. Optical microscopy images of the Cu layers electrodeposited at (a) 0 and (b) −50 mV. SEM images of the Cu layers electrodeposited at (c) −100, (d) −200, (e) −400, and (f) −600 mV. Arrows refer to the growth center and the dotted line refers to the branch shape.

slope of −0.5, which was reported in the relation between current and time in the Cottrell equation. Therefore, the applied potential can be divided into two categories: kinetic control and diffusion control.

Figure 2 shows the surface images of the Cu layers electrodeposited at various applied potentials. As shown in Figs. 2a and 2b, the Cu layers formed at 0 and −50 mV, respectively, did not fully cover the Mo substrate, even after the termination of the process, as expected in the chronoamperometry result. On the other hand, the Mo substrates were completely covered with the Cu layers when the potentials of −100 and −200 mV corresponding to the kinetic controlled reaction were applied for the reduction. Interestingly, in these potentials, several branches seemed to be grown from the same nuclei centers. The number of growth centers was increased with increasing negative potential, as indicated in Figs. 2c and 2d. However, for potentials that were more negative than −400 mV corresponding to the diffusion controlled region, branch shape was not observed; instead, the island shaped protrusions were formed, as shown in Figs. 2e and 2f.

Moreover, no significant change in the surface morphology was found in the potential of −400 ∼ −600 mV. It is considered that these islands are agglomerated Cu at local points. Consequently, the surface morphology of Cu was determined according to the reaction type during the electrodeposition, and the deposition in the diffusion controlled region induces a similar morphology.

For the formation of the reproducible and uniform $CuInSe_2$ and/or $Cu(In_xGa_{1-x})Se_2$ absorber layers, the electrodeposited metallic layers in the multistacked precursors should have uniform and smooth surfaces for the homogenous distribution of each metallic ion after the selenization process at high annealing temperatures. However, as shown in Fig. 2, the Cu films grown in kinetically controlled and diffusion controlled regions have dendritic surface and agglomerated Cu phases, respectively. Consequently, for the potentiostatically deposited Cu layers in the electrolyte, these non-uniform surfaces are expected to induce the irregular distribution of Cu elements in an absorber layer after the selenization. In particular, the rough Cu layers are considered to cause a preferred formation of thermodynamically stable Cu_2Se phases in the initial stage of thermal annealing, which is known to induce the leakage current path degrading the fill factor and the conversion efficiency of solar cells due to their semi-metallic characteristics.[28] Thus, D. Mercier et al. suggested commercial organic additives composed of polyethylene glycol, bis(3-sulfopropyl)disulfide, and Janus Green B in order to enhance the surface roughness of the Cu layer.[29] Alternatively, in our study, we employ a two-step process designed for the deposition of the uniform Cu layers, which is performed by the in-situ control of applied potential without organic additives.

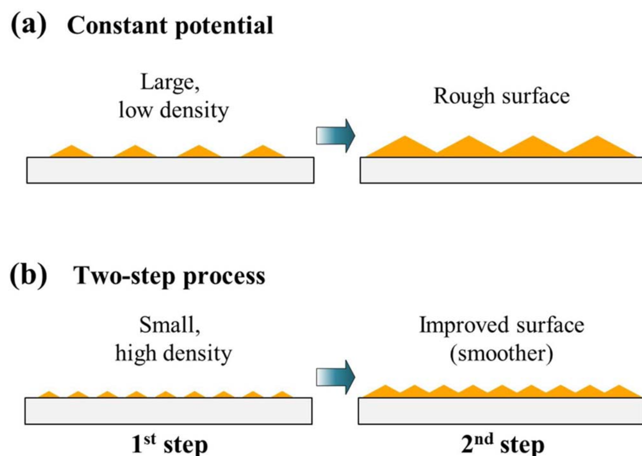

Figure 3. Schematic diagrams for growth evolution of electrodeposited Cu layers: (a) constant potential and (b) two-step process.

Figure 3 shows a schematic diagram for the two-step process, where this model is suggested on the basis of the results of Figs. 1 and 2. Similar to the thin film growth mechanism, well-organized in the formation of the heterogeneous layers using the vacuum process, high density Cu nuclei with small size were produced in the first step, and these nuclei were then coalesced at the second step, promoting a smooth surface. This deposition process is expected to readily induce smoother heterogeneous films since the high density of the nuclei induces a close distance between the nuclei and a fast coalescence step, resulting in the smooth surface. For the chemical vapor deposition process, the two-step process using a nucleation layer has now become a standard method for the heterostructure growth with high quality, and growth temperature and reactor pressure were the main parameters for the control of the growth mechanism. On the other hand, for the electrodeposition process, the two-step process is still an unfamiliar method. However, among various deposition parameters, applied potential is certainly the most important parameter to influence growth condition and behavior of the hetero layers. For example, two-step metallorganic chemical vapor deposition was first developed for growing the GaN epilayers on sapphire substrates for light emitting diode fabrication. A very thin nucleation layer of GaN or AlN was grown at a low temperature, followed by high temperature process to enhance the lateral growth. This result was a technical breakthrough in high-quality GaN film growth.[31] Similarly, we attempted to deposit the two-step processed Cu layers to improve the surface roughness, with the control of applied potentials, as shown in Figs. 5 and 6. Firstly, to obtain the high nuclei density of Cu, the potential was varied from

Downloaded on 2016-03-14 to IP 115.145.248.215 address. Redistribution subject to ECS terms of use (see ecsdl.org/site/terms_use) unless CC License in place (see abstract).

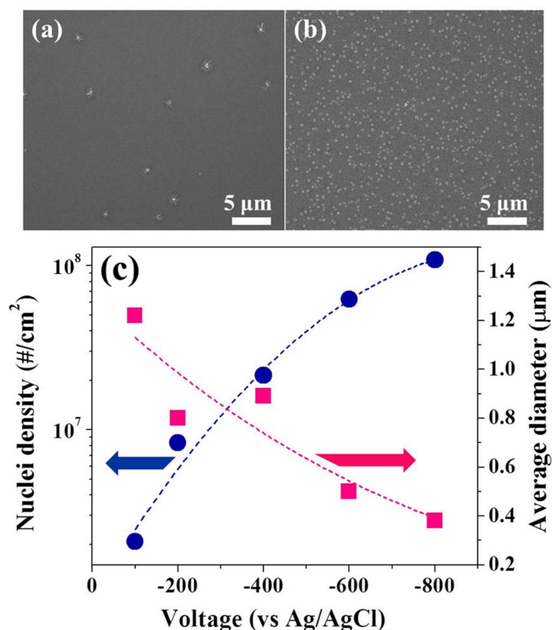

Figure 4. SEM images of Cu nuclei formed at (a) −100 and (b) −800 mV for a short period of time (0.5 sec). (c) Changes in areal density and average diameter of Cu nuclei formed at various potentials (−100, −200, −400, −600, and −800 mV) for a short period of time (0.5 sec).

−100 to −800 mV for a very short period of time (0.5 sec), regardless of the diffusion controlled reaction at ≤ −400 mV [Fig. 1c]. As shown in Fig. 4c, the density of Cu nuclei in the initial stage was continuously increased from $\sim 2 \times 10^6$ to $\sim 1 \times 10^8$/cm^2, while the potential was changed from −100 to −800 mV. In contrast, the average diameter of Cu nuclei was decreased from 1.22 µm (−100 mV) to 0.38 µm (−800 mV). Consequently, a further negative potential is preferred to obtain the nuclei with high density and small diameter as the first step of the two-step process.

An applied potential for the second step was selected as −100 mV, which showed kinetic controlled reaction because the stabilized current in the final stage indicating the formation of films was observed at this potential, as shown in Fig. 1c. Diffusion controlled reaction at the second step could produce the agglomerated Cu phases, similarly to the morphology shown in Figs. 2e and 2f. Figure 5 shows the chronoamperometry result for the two-step process, where −800 mV was applied at the first step and the potential of −100 mV was applied after the nucleation step. This result was compared with the current-time transient of the Cu layer grown with a single step under −100 mV. The reduction current density was rapidly increased when −800 mV was applied on the Mo substrate in the first step. The current density was then decreased due to the growth and some coalescence of Cu nuclei for 0.5 sec. Next, the potential change into −100 mV for the second step induces an abrupt decrease in current density. Interestingly, a further decrease in current density was observed during the deposition at the second step because additional growth and coalescence of Cu nuclei occurred in the second step. This result indicates

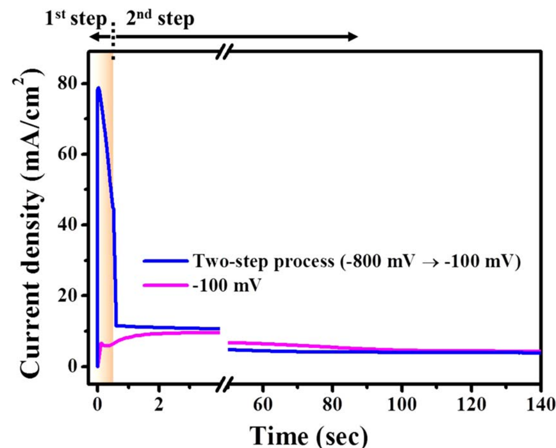

Figure 5. Comparative results of chronoamperometry curves for the Cu electrodeposited at constant potentials (−100 mV) and two-step process (−800 mV → −100 mV).

that 0.5 sec was an insufficient length of time to form the fully coalesced layer, and the coalescence of nuclei and the formation of films mainly occurred in the second step. In particular, the current density in the two-step process was stabilized earlier than the deposition at constant potential, −100 mV. Consequently, it is assumed that the two-step process having the high density of nuclei leads to continuous film growth in a shorter period of time due to the acceleration of the coalescence process of the nuclei, as expected.

Table I shows the experimental conditions used to compare the surface morphology of the Cu layers with similar thicknesses. Samples 1 and 2 were deposited at constant potentials of −100 and −600 mV, which correspond to the kinetic and diffusion controlled growth regions, respectively. Meanwhile, samples 3 and 4 were fabricated using the two-step process. The applied potentials in the first step of samples 3 and 4 were −600 and −800 mV, respectively, for the high nucleation density. The surface roughness of these samples was quantified by images and linear profiles of the non-contact mode AFM, as shown in Fig. 6. Figures 6a, 6c, 6e, and 6g show the topography of these Cu layers grown on Mo substrates to visually confirm the surface morphology. The roughness profiles were obtained along the dotted lines in the topography, as shown in Figs. 6b, 6d, 6f, and 6h. As shown in Fig. 6b, a significant difference in height was observed when Cu was electroplated using the potentiostatic deposition method at −100 mV, where the height difference is above 400 nm. This difference decreased when Cu was grown at a more negative potential, −600 mV. Unfortunately, the height difference is still high and the distance between the maximum heights is narrow due to the formation of island shaped agglomerates. Interestingly, the introduction of the two-step process clearly resolves these problems, as shown in Figs. 6f and 6h. Root mean square (RMS) values of each sample calculated from the same area were quantified from the AFM images, as shown in Fig. 7a. As a result, the RMS value decreased from 23.0 to 12.1 nm by the change of applied potential from −100 to −600 mV, respectively, and finally showed an abrupt decrease of 6.0 nm in the two-step process in sample 4. Among the two-step processed samples, more

Table I. Experimental conditions for electrodeposited Cu layers and Cu/In structures.

sample no.	Cu plating		In plating	
1	Constant potential	−100 mV	Constant potential	−680 mV
2	Constant potential	−600 mV	–	–
3	Two-step	−600 mV (0.5 sec) → −100 mV	–	–
4	Two-step	−800 mV (0.5 sec) → −100 mV	Constant potential	−680 mV

Downloaded on 2016-03-14 to IP 115.145.248.215 address. Redistribution subject to ECS terms of use (see ecsdl.org/site/terms_use) unless CC License in place (see abstract).

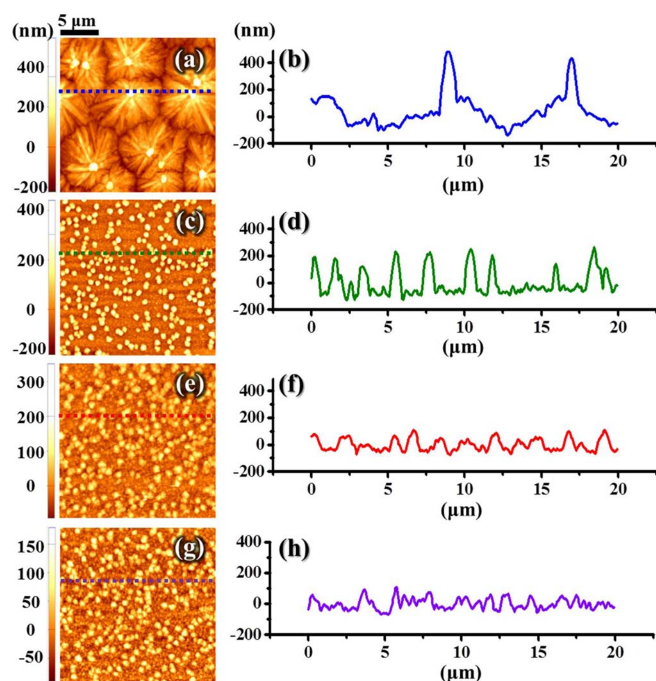

Figure 6. Topography images and line profiles of Cu layers measured using AFM: (a, b) −100 mV, (c, d) −600 mV, (e, f) two-step process (−600 mV → −100 mV), and (g, h) two-step process (−800 mV → −100 mV).

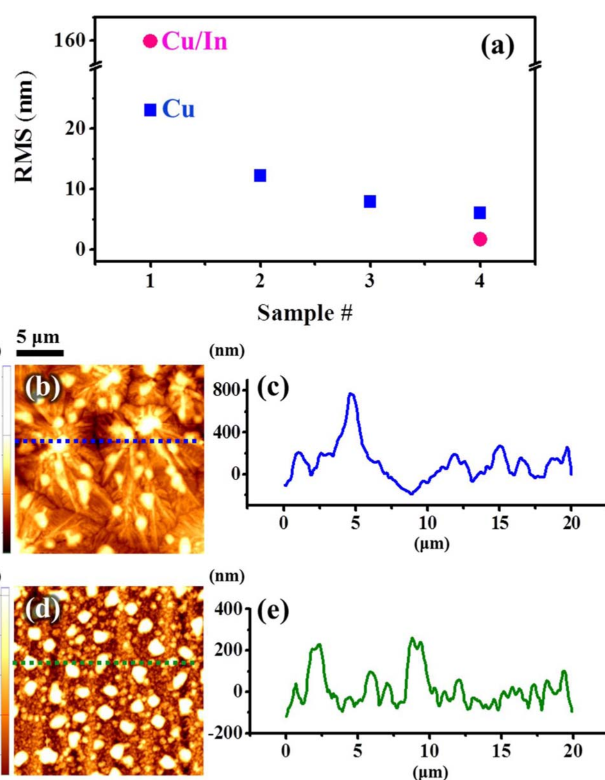

Figure 7. (a) RMS values for the samples prepared by growth conditions shown in Table I. Topography images and line profiles of Cu/In stacked structure measured using AFM: (b, c) sample 3 and (d, e) sample 4.

negative potential at the first step induced the lower RMS value in all the Cu layers. This result suggests the conclusion that the two-step process is a convenient method to authentically improve the surface roughness of the electrodeposited Cu layers, as suggested in Fig. 3.

In electrodeposition, the surface shape of the working electrode is one of the key parameters determining the reaction behavior, since the reduction process occurs at the interface between the working electrode's surface and electrolyte. The rough surface could induce the different distributions of reaction current density, and thus the protrusion on the surface induces an excess of current density compared to the planar surface.[32,33] Accordingly, the underlying layers play the role of a working electrode for the deposition of subsequent reactants in multistacked structures such as Cu/In and Cu/In/Ga films. Thus, we electrodeposited an In layer on the Cu surface of samples 1 and 4 to determine the effects of surface roughness of the Cu underlying layers. For the In coating, a 200 mC/cm^2 charge was delivered, which corresponds to ∼100 nm thickness. Here, the applied potential of −680 mV was maintained. As a result, the In deposition on sample 1 having a large difference in height shows a drastic increase of a RMS value up to 160 nm, as shown in Figs. 7a, 7b, and 7c. In particular, the highest points in the surface roughness of the Cu/In bilayers correspond to the highest points of the Cu layers [Fig. 7b]. On the contrary, the In electrodeposition in sample 4 showed a slight decrease in areal RMS values, even after the In deposition, as shown in Fig. 7a.

Based on the experimental results, we can propose schematic models to clearly show the growth evolution of the Cu/In bilayers, as shown in Fig. 8. The general phenomenon is known in which sharp edges on the surface can induce a local high current density during the electrodeposition.[32,33] Consequentially, the significant increase of height difference due to the In deposition in sample 1 is because a higher current density in the In reduction process flows through the protrusion regions of the Cu layers (growth center) [Fig. 8a], resulting in quite rough Cu/In bilayer films. On the contrary, for the Cu layer having reduced roughness, a uniform current density is expected to be applied on the entire surface, and as a result, the relatively smooth In layer could be coated on the Cu. Consequently, two-step process electrodeposition induces a relatively improved surface for the Cu and Cu/In stacked layers. This method is also expected to provide a

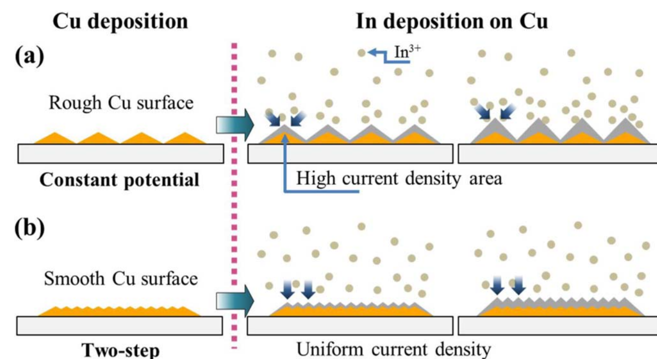

Figure 8. Schematic models showing the growth evolution of the Cu/In bilayers.

feasible strategy for the reproducible and uniform formation of the Cu-In system based absorbers.

Conclusions

The Cu and Cu/In layers were prepared from an artificially controlled electrodeposition system for the formation of solution processed multistacked metal precursors in CIGS solar cells. In electrodeposition using an ionic solution, the rough surface of the underlying layers could be exploited as templates for the coating of the subsequent metal layers. Consequently, the rough surface induces a more serious surface morphology due to the locally different potential distributions. The Cu layers prepared at a constant potential showed a limit in overcoming the problem related to surface roughness, because both kinetic controlled and diffusion controlled depositions induced a significant difference in the its height. Therefore, the two-step process was designed to modify the surface roughness in the

Downloaded on 2016-03-14 to IP 115.145.248.215 address. Redistribution subject to ECS terms of use (see ecsdl.org/site/terms_use) unless CC License in place (see abstract).

electrodeposition of the Cu layer. In the two-step process, a high density of Cu nuclei was formed at the first step and these were coalesced at the second step. As a result, the surface roughness of the Cu layer was considerably improved, and the In coated on this layer also exhibited a significantly improved surface.

Acknowledgments

This work was supported by the National Research Foundation of Korea (NRF) grant funded by the Korea government (MSIP) (NRF-2012R1A2A4A01003849), (2014R1A4A1008474) and (NRF-2012-0001262). This work was also supported by the Energy International Collaboration Research & Development Program of the Korea Institute of Energy, Technology and Planning (KETEP) funded by the Ministry of Knowledge Economy (MKE) (2011-8520010050).

References

1. P. Jackson, D. Hariskos, E. Lotter, S. Paetel, R. Wuerz, R. Menner, W. Wischmann, and M. Powalla, *Prog. Photovoltaics*, **19**, 894 (2011).
2. P. Reinhard, S. Buecheler, and A. N. Tiwari, *Sol. Energ. Mat. Sol. C.*, **119**, 287 (2013).
3. S. C. Riha, B. A. Parkinson, and A. L. Prieto, *J. Am. Chem. Soc.*, **131**, 12054 (2009).
4. K. L. Chopra, P. D. Paulson, and V. Dutta, *Prog. Photovoltaics*, **12**, 69 (2004).
5. X. Z. Wu, *Sol. Energy*, **77**, 803 (2004).
6. H. Katagiri, *Thin Solid Films*, **480**, 426 (2005).
7. H. Katagiri, K. Jimbo, W. S. Maw, K. Oishi, M. Yamazaki, H. Araki, and A. Takeuchi, *Thin Solid Films*, **517**, 2455 (2009).
8. I. Repins, M. A. Contreras, B. Egaas, C. DeHart, J. Scharf, C. L. Perkins, B. To, and R. Noufi, *Prog. Photovoltaics*, **16**, 235 (2008).
9. P. Jackson, D. Hariskos, R. Wuerz, W. Wischmann, and M. Powalla, *Phys. Status Solidi RRL*, **8**, 219 (2014).
10. S. Taunier, J. Sicx-Kurdi, P. P. Grand, A. Chomont, O. Ramdani, L. Parissi, P. Panheleux, N. Naghavi, C. Hubert, M. Ben-Farah, J. P. Fauvarque, J. Connolly, O. Roussel, P. Mogensen, E. Mahé, J. F. Guillemoles, D. Lincot, and O. Kerrec, *Thin Solid Films*, **480–481**, 526 (2005).
11. R. N. Bhattacharya, *Sol. Energ. Mat. Sol. C.*, **113**, 96 (2013).
12. A. Duchatelet, T. Sidali, N. Loones, G. Savidand, E. Chassaing, and D. Lincot, *Sol. Energ. Mat. Sol. C.*, **119**, 241 (2013).
13. K. T. Ramakrishna Reddy, N. Koteswara Reddy, and R. W. Miles, *Sol. Energ. Mat. Sol. C.*, **90**, 3041 (2006).
14. A. Mittiga, E. Salza, F. Sarto, M. Tucci, and R. Vasanthi, *Appl. Phys. Lett.*, **88**, 163502 (2006).
15. J. Puthussery, S. Seefeld, N. Berry, M. Gibbs, and M. Law, *J. Am. Chem. Soc.*, **133**, 716 (2011).
16. E. J. Luber, M. H. Mobarok, and J. M. Buriak, *ACS Nano*, **7**, 8136 (2013).
17. L. Isac, A. Duta, A. Kriza, S. Manolache, and M. Nanu, *Thin Solid Films*, **515**, 5755 (2007).
18. L. Lahourcade, N. C. Coronel, K. T. Delaney, S. K. Shukla, N. A. Spaldin, and H. A. Atwater, *Adv. Mater.*, **25**, 2562 (2013).
19. D. O. Scanlon and A. Walsh, *Appl. Phys. Lett.*, **100**, 251911 (2012).
20. P. Zhao and S. Cheng, *Adv. Mater. Sci. Eng.*, **2013**, 4 (2013).
21. Q. Guo, G. M. Ford, H. W. Hillhouse, and R. Agrawal, *Nano Lett.*, **9**, 3060 (2009).
22. M. G. Panthani, V. Akhavan, B. Goodfellow, J. P. Schmidtke, L. Dunn, A. Dodabalapur, P. F. Barbara, and B. A. Korgel, *J. Am. Chem. Soc.*, **130**, 16770 (2008).
23. M. Kaelin, D. Rudmann, and A. N. Tiwari, *Sol. Energy*, **77**, 749 (2004).
24. S. Ahn, K. H. Kim, J. H. Yun, and K. H. Yoon, *J. Appl. Phys.*, **105**, 113533 (2009).
25. J. C. Malaquias, M. Steichen, M. Thomassey, and P. J. Dale, *Electrochim. Acta*, **103**, 15 (2013).
26. D. Lincot, J. F. Guillemoles, S. Taunier, D. Guimard, J. Sicx-Kurdi, A. Chaumont, O. Roussel, O. Ramdani, C. Hubert, J. P. Fauvarque, N. Bodereau, L. Parissi, P. Panheleux, P. Fanouillere, N. Naghavi, P. P. Grand, M. Benfarah, P. Mogensen, and O. Kerrec, *Sol. Energy*, **77**, 725 (2004).
27. S. M. Lee, S. Ikeda, T. Yagi, T. Harada, A. Ennaoui, and M. Matsumura, *Phys. Chem. Chem. Phys.*, **13**, 6662 (2011).
28. S. Yoon, T. Yoon, K.-S. Lee, S. Yoon, J. M. Ha, and S. Choe, *Sol. Energ. Mat. Sol. C.*, **93**, 783 (2009).
29. D. Mercier, E. Delbos, H. El Belghiti, J. Vigneron, M. Bouttemy, and A. Etcheberry, *J. Electrochem. Soc.*, **160**, D3103 (2013).
30. D. Grujicic and B. Pesic, *Electrochim. Acta*, **47**, 2901 (2002).
31. X. H. Wu, L. M. Brown, D. Kapolnek, S. Keller, B. Keller, S. P. DenBaars, and J. S. Speck, *J. Appl. Phys.*, **80**, 3228 (1996).
32. K. M. Takahashi and M. E. Gross, *J. Electrochem. Soc.*, **146**, 4499 (1999).
33. J.-M. Quemper, S. Nicolas, J. P. Gilles, J. P. Grandchamp, A. Bosseboeuf, T. Bourouina, and E. Dufour-Gergam, *Sensor. Actuat. A-Phys.*, **74**, 1 (1999).

Downloaded on 2016-03-14 to IP 115.145.248.215 address. Redistribution subject to ECS terms of use (see ecsdl.org/site/terms_use) unless CC License in place (see abstract).